RSC Advances

This is an *Accepted Manuscript*, which has been through the Royal Society of Chemistry peer review process and has been accepted for publication.

Accepted Manuscripts are published online shortly after acceptance, before technical editing, formatting and proof reading. Using this free service, authors can make their results available to the community, in citable form, before we publish the edited article. This *Accepted Manuscript* will be replaced by the edited, formatted and paginated article as soon as this is available.

You can find more information about *Accepted Manuscripts* in the Information for Authors.

Please note that technical editing may introduce minor changes to the text and/or graphics, which may alter content. The journal's standard Terms & Conditions and the Ethical guidelines still apply. In no event shall the Royal Society of Chemistry be held responsible for any errors or omissions in this *Accepted Manuscript* or any consequences arising from the use of any information it contains.

ROYAL SOCIETY OF CHEMISTRY

www.rsc.org/advances

Structure-Property Relationship and Interfacial Phenomena in GaN Grown on C-plane Sapphire via Plasma-Enhanced Atomic Layer Deposition

P. Motamedi and K. Cadien

Department of Chemical and Materials Engineering, University of Alberta, Edmonton, Alberta, Canada T6G 2V4

Keywords: ALD, PEALD, GaN, growth, structure, properties

RSC Advances Accepted Manuscript

Abstract

Gallium nitride films were deposited via plasma-enhanced atomic layer deposition (PEALD) using triethylgallium and forming gas as precursors. An optimized process was developed and the effect of growth temperature on the structure and optical properties of the films investigated. In-depth X-ray diffraction analyses show that there is a critical temperature, below which the films are amorphous. Raising the growth temperature above the critical temperature increases the grain size of the polycrystalline film, while degrading the degree of preferred orientation. Azimuthal XRD scans show clear signs of crystallographic relationship between the (002) planes of the sapphire substrate and GaN. Growth rate shows a steady rise until a rapid jump at 425°C occurs. The study of the surface profile by AFM shows that the hillocks on the surface start to grow in diameter as well as height, increasing the total growth front area. This also decreases the surface roughness. XRR studies reveal that mass density reaches its maximum value at 240°C, and is stable after that. Carrier mobility is increased by two orders of magnitude, when the growth temperature is raised from 150°C to 425°C. As expected, a similar but reverse trend was observed for the electrical resistivity. Refractive index follows the trends of mass density and crystal quality with a clear increase at the onset of crystallinity. Overall, the surface profile and the engineering properties improve as growth temperature is increased. At the high end of the growth temperature range, PEALD GaN films grown on (002) sapphire were p-type with a hole mobility of 575 cm^2/vs.

RSC Advances Accepted Manuscript

1. Introduction

Gallium nitride (GaN) is a direct band gap semiconductor with good chemical and thermal stability that make it a suitable choice for many engineering applications, such as laser diodes, light-emitting diodes and sealed devices and environmental sensors[1-6]. High Young's modulus makes GaN more appropriate than silicon for resonant devices[5,7], and the pyroelectric properties of GaN offer possibilities for MEMS and NEMS energy harvesting devices with novel functionalities[8,9].

GaN has been grown by metal-organic chemical vapor deposition[1–3], reactive sputtering[4,5], molecular beam epitaxy[6,7], and pulsed laser deposition[8,9]. However, there does not appear to be a well-researched method capable of producing crystalline GaN thin films with preferential orientation at low growth temperatures. Atomic layer deposition (ALD) offers exceptional control over the film thickness, conformality, scale-up potential, and considerably lower deposition temperatures[10,11]. There are several studies on the effect of growth temperature on the properties of ALD films [12–18]. A survey of this literature shows that even when the chemical reactions of the deposition and the physical structure of the films are similar, changing the growth temperature can lead to diverse and even contrasting results. The results of the initial research on the ALD of GaN has been recently published[19–21]. However, to date, there is no report on a comprehensive study of the effect of substrate temperature on the growth mechanism, structural evolution, and electrical properties of GaN grown on sapphire.

This paper reports on the effect of substrate temperature on the plasma-enhanced ALD (PEALD) growth mechanism, structural evolution, and electrical properties of GaN, and paves the way for engineering GaN thin films with targeted properties. A comprehensive analysis of

RSC Advances Accepted Manuscript

the crystal structure, variations of the growth rate and a possible relationship with the changes of the surface roughness is presented. The effect of these structural changes on electrical resistivity, carrier mobility and refractive index of the films are discussed.

2. Experimental Section

GaN films were deposited in an atomic layer deposition research system (ALD-150LX, Kurt J. Lesker) equipped with an in situ J. A. Woollam M-2000DI ellipsometer with a fixed angle of 70° that has been described in detail elsewhere[22]. Triethylgallium (TEG) was used as the gallium precursor, and remote forming gas plasma (600 W), with a nitrogen to hydrogen ratio of 19:1, was used as the other precursor. Pulse width and purge times were optimized to achieve a saturated ALD process. All films were grown on sapphire (002) substrates. Samples were deposited at actual substrate temperatures of 150°, 200°, 240°, 275°, 325°, 360°, and 425°C, rounded to the nearest 5°C. These temperature values represent the heater set point temperature corrected by calibrations that were done to determine the actual substrate surface temperature versus heater temperature. All deposition parameters except for the substrate temperature were kept constant for the samples. All substrates were exposed to N_2/H_2 plasma for 60 seconds, in order to clean and condition the substrate surface, immediately prior to the initiation of deposition.

The growth rate and film thickness were collected from in-situ spectroscopic ellipsometry data. In order to isolate the effect of temperature on the complex dielectric function, total film thickness was derived from ex-situ measurements at room temperature, and in-situ measurements were exclusively used to study the effect of film thickness on optical properties. X-ray diffraction (XRD) and X-ray reflectometry (XRR) measurements were carried out using a

RSC Advances Accepted Manuscript

Bruker-AXS D8-Discover machine with a Cu Kα source ($K\alpha_2$ was removed before analysis). XRD data were collected using a Vantec 500 2-D detector and GADDS software, and analyzed using EVA software. XRR data and azimuthal scans were recorded using a NaI scintillometer. Commander D8 and Leptos programs were used for data acquisition and analysis, respectively. A Bruker Dimension-Edge AFM system was used to map the sample surface. Silicon tips were used in tapping mode, and the amplitude set point was 2.4 V. AFM results were analyzed using Bruker Nanoscope Analysis 1.5 software. Hall effect measurements were done using a Nanometrics HL5500 system operated at 0.01 μA.

3. Results and Discussion

3.1. Deposition Mechanism

The ALD simplified half and overall reactions are given below,

$$Ga(C_2H_5)_3 + H^* \rightarrow Ga(C_2H_5)_2^* + C_2H_6 \quad (1)$$

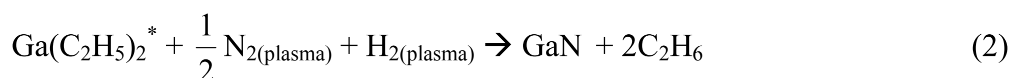

$$Ga(C_2H_5)_2^* + \frac{1}{2}N_{2(plasma)} + H_{2(plasma)} \rightarrow GaN + 2C_2H_6 \quad (2)$$

Overall,

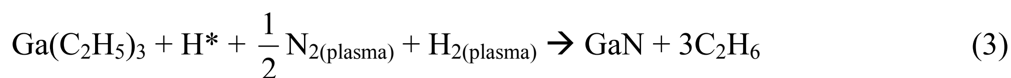

$$Ga(C_2H_5)_3 + H^* + \frac{1}{2}N_{2(plasma)} + H_{2(plasma)} \rightarrow GaN + 3C_2H_6 \quad (3)$$

where * indicates the atom/molecule is on the surface.

In order to establish the optimal deposition parameters for the ALD growth of GaN under saturated ALD conditions, the variation of growth rate (growth per cycle, GPC), measured by X-ray reflectometry, was studied as a function of the precursor pulse width as shown in Fig.1. For both precursors, the growth rate saturates as the pulse width increases. This is indicative of a self-limited growth regime, which is typical of atomic layer deposition. Based on these studies, a

RSC Advances Accepted Manuscript

single growth cycle consisted of four segments: 0.04s TEG exposure, 7s Ar purge, 15s N_2/H_2 plasma exposure, and 7s Ar purge.

3.2. Crystal Structure

Two-dimensional X-ray diffraction was used to analyze the crystal structure of the films. A schematic diagram of the test setup is shown in Fig. 2. The angle between the source and the detector is 2θ, and the Cartesian coordinates relative to the sample surface x, y and z are shown and the rotations around these axes are χ, ω and φ, respectively. The detector collects data in a window of θ and χ angles. For the settings used, the output data is in the form of an image, in which 2θ increases from 32° to 43° (the location of the GaN (002) peak), while χ changes along the arcs centered at 2θ = 0°. At 2θ = 36° and χ increases from -99° to -81°. The imaginary horizontal line passing through the center of the image indicates χ = -90°. These images are the results of the data recorded while ω was scanned from 15° to 28°, and 2θ was kept constant at 34°. Under these conditions, random out-of-plane orientation creates cones of diffracted x-rays, which are intercepted by the detector, and revealed as rings with a uniform radial intensity distribution[23]. Therefore the degree of radial nonuniformity in the image is a measure of crystal order[24,25]. Fig. 3 shows the two-dimensional XRD frames.

All the images feature a bright dot at 2θ = 41.6°, which corresponds to the sapphire (006) reflection. The fact that this diffraction creates a dot with a very narrow distribution along χ indicates that the (006) reciprocal lattice vector becomes coplanar with the beam vector only at χ = -90. This is expected from a single crystal wafer. Study of Fig. 3 shows that no significant trace of GaN crystals is detected at 240°C and below. At 275°C (Fig. 3-d), a bright dot appears at 34.4°. This corresponds to the GaN (002) reflection. The absence of (100) and (101) reflections

RSC Advances Accepted Manuscript

indicates a preferential growth orientation along the (002) plane normal. At this temperature, the pattern looks similar to that of a single crystal. At higher deposition temperatures, the (002) dot keeps getting brighter, while an arc appears at 2θ = 36.9°, and corresponds to GaN (101) reflection. At 425°C the (101) dot shows a significant increase in intensity and the brightness is more concentrated at the central point of the arc, but the (101) arc is also more noticeable. The fact that the (101) intensity is distributed along an arc necessitates the integration of data over lines and arcs for comparison. Fig. 4 shows the results of integration over χ along 2θ and confirms that there is no measurable GaN crystallinity at 240°C and below. The strongest (002) preferential orientation is observed at 275°C, while at higher temperatures the (101)/(002) peak intensity ratio keeps rising. The degree of preferential orientation along χ is shown in Fig. 4b, where all the samples deposited at and above 275°C show strong peaks at χ = -90°. In general, the preferential orientation is maintained or improved with increasing temperature, with the exception of the sample deposited at 360°C, in which a slightly wider distribution is observed.

Careful examination of χ-integrated spectra shows that the position of the GaN (002) peak does not show a meaningful change, when the deposition temperature varies. The peak position of 34.4° translates into the interplanar distance of 0.271 nm, which when compared to the commercial fully relaxed wafers tested under the same conditions, results in ε_{cc}, the strain along the c-axis, being 0.0032. Eq. (4) shows the relationship among strain along *a* and *c* axes, and υ, Poisson's ratio. According to this equation, and considering a value of 0.183 for ϑ[26], this translates into ε_{aa}= 0.0071, and σ_{aa}=2.5 GPa, which does not seem to vary with deposition temperature, in the range tested here.

$$\frac{\varepsilon_{cc}}{\varepsilon_{aa}} = \frac{-2\vartheta}{1-\vartheta} \tag{4}$$

RSC Advances Accepted Manuscript

While a transition from amorphous to crystalline films has been reported before for ALD deposited semiconductors [13,14,27,28], the further changes of crystal structure observed after the onset of crystallinity at 275°C is not commonly reported. Yuan et al.[17] have reported the tendency of ALD ZnO grown on glass to lose preferential orientation at higher temperature, which is the more extreme case of what we observed for GaN between 275° and 425°C. Since both studies show an increased growth rate at higher temperatures, this may explain the randomization of crystal orientation, that is, the higher growth rate leaves less time for the atoms to relocate and minimize their surface energy, which is the root cause of the (002) preferential orientation.

A quantitative comparison of the peak intensities among different samples was not undertaken, because in thin films with strong preferential orientation, the diffraction intensity of the planes parallel to the surface is extremely sensitive to sample orientation. The maximum intensity is achieved, when the beam vector and surface normal are exactly coplanar, and that is rarely the case in practice. The effect of this misorientation was demonstrated in the ϕ-scan as shown in Fig. 5. The top spectrum shows the (006) reflection of sapphire and the lower spectrum shows the (002) reflection of GaN with the ω angle set at 20.8° and 17.2°, respectively. 2θ was kept constant at twice the mentioned values, while the sample was rotated 360° around the surface normal. The two independently recorded spectra were then superimposed for comparison. The large variation in the intensity vs. ϕ is evident and is due to the noncoplanarity of the beam vector and the surface normal. Since the exact coplanarity angle can only be detected using a scintillometer, the XRD spectra featured in Fig. 4a recorded with a two-dimensional detector

RSC Advances Accepted Manuscript

cannot be used for a quantitative comparison of (002) peak intensities. Another noteworthy feature of Fig. 5 is the fact that the two spectra show maxima at the same ϕ values. This is an indication that the normal to the sapphire (006) plane and GaN (002) plane are aligned[29] and proof of a crystallographic relationship between the two lattices.

Considering the above discussion, any valid comparison between the samples should be performed when the peak intensity is at its maximum value. XRD rocking curves of GaN (002) peaks were used for this purpose. A ϕ-scan was performed individually for each sample, then ϕ was set at the value that provided the coplanarity condition. The rocking curves were then recorded under this condition, while 2θ was set at the peak position, and the variation of intensity vs. ω was recorded, as shown in Fig. 6. Analysis of the spectra reveals that the FWHM remains constant, while the peak intensity varies among the samples. This indicates that the distribution of interplanar distances remains unchanged for the samples, while the total diffraction intensity increases with increasing temperature. The intensity drop from 325° to 360°C could be an indication of either lower crystallinity or weaker preferential orientation of the sample deposited at 360°C. As seen, the intensity at 425°C is markedly higher than all other samples. This is due to contributions from the degree of crystallinity, the preferential orientation, and the higher growth rate at this temperature, as discussed in Section 3.3.

3.3. Growth Mechanism and Thin Film Structure

The values of the film thickness were recorded via spectroscopic ellipsometry, and are listed in Table 1. Based on these values, the variation of the growth rate versus temperature and the reciprocal of the absolute growth temperature, is plotted and shown in Fig. 7. A steady rise in the growth rate is observed, for temperatures up to 360°C. An increase in the kinetic energy of the

RSC Advances Accepted Manuscript

reactants is deemed responsible for this increase. This result also indicates that the known mechanisms for the potential decrease in ALD growth rate with increasing substrate temperature are either not activated or their effects are not strong enough to overcompensate for the increased kinetic energy. In other words, no significant premature dissociation of the precursors or desorption of the deposited material occur within this temperature range.

Table 1: The values of film thickness and the number of monolayers for the films deposited at different temperatures§

Growth temperature (°C)	**Film thickness (Å)**	**Number of monolayers**
150	399	154
200	452	175
240	525	203
275	557	215
325	587	227
360	637	246
425	944	364

§ All the films have gone through 1000 cycles of deposition.

The general trend of increasing growth rate with temperature has been reported earlier for temperatures below 500°C [19,20]. Considering the fact that the temperature of the precursor lines and the chamber walls are less than 150°C, which is well below the homogenous pyrolysis temperature of TEG[30,31], homogeneous decomposition is ruled out. Donnelly and coworkers[32,33] have conducted mass spectrometric studies of thermal decomposition of adsorbed TEG on GaAs. They reported that at higher temperatures (>300°C) a greater portion of the decomposition

RSC Advances Accepted Manuscript

products consists of hydrocarbons, and that Ga atom sticking probability increases. If a similar trend exists for GaN it could contribute to ALD growth, and lead to higher growth rates at elevated substrate temperatures. As seen in Fig. 7, a large jump in the growth rate is observed for deposition at 425°C, which does not fit the aforementioned exponential trend. A survey of the literature shows that some authors have suggested that an increase in ALD growth rate at higher temperatures is due to "CVD-like reactions", hence ruling them out as ALD depositions, solely based upon the growth rate[15,27]. In the case of the ALD of GaN using TEG, the homogeneous pyrolysis of TEG is not favorable. In addition, any CVD-like reaction among the products of pyrolysis would compromise the structural integrity of the films. This would manifest itself in the form of disturbed crystal order, lower mass density, and lower carrier mobility. None of these symptoms were observed for the films grown at 425°C. Furthermore, in the case of pyrolysis and CVD-like reactions, there would be no constraint that limits the growth rate to the characteristic sub-monolayer-per-cycle growth rate of ALD. For the films under study in this paper, even after the growth rate jump at 425°C, the growth rate is less than 0.5 ML/cycle, which is typical for ALD reactions. Therefore, explanation of the high growth rate at 425°C requires a comprehensive and multifaceted approach that will be discussed later, in light of XRD and AFM studies.

Atomic force microscopy was employed to measure the average surface roughness of the films, as shown in Fig. 8. The roughness increases with growth temperature and reaches a maximum at 360°C, before it starts to decrease. It is important to note that in our studies surface roughness was found to increase with film thickness. . Considering the fact that GPC at 425°C is 48% higher than that of 360°C and that the two films have the same number of ALD cycles, the sample deposited at higher temperature is thicker and expected to have higher surface roughness,

RSC Advances Accepted Manuscript

yet the opposite is observed. In order to understand this, the changes of the surface morphology must be investigated. Fig. 9 shows the AFM images from the surface of three films deposited for 1000 cycles at different temperatures. At 150°C the surface of the film is mostly two-dimensional with occasional sporadic bumps. The 360°C landscape is markedly different, as the entire surface is covered with sharp hillocks of high aspect ratio. The average roughness is therefore expected to be substantially higher than Fig. 9a. In contrast to this trend, in Fig. 9c the surface bumps have become thicker, and show a smaller aspect ratio. It appears that the bumps have a tendency to grow in diameter, as well as height. A good understanding of this behavior needs knowledge about the crystal structure and the nature of the crystallographic directional growth in the films.

Comprehensive XRD studies (Figs. 3-6) have shown that the reciprocal lattice vector is parallel to the substrate (001) normal. As a result, the increase in the hillock aspect ratios, demonstrated by the increasing roughness, is due to accelerated growth in the [001] crystallographic direction. Similarly, a decrease in aspect ratio indicates an accelerated growth along <100> and <101> directions. The fact that this acceleration occurs at higher temperatures means it is temperature induced, and has a higher activation energy than that of the [001] direction. Gu et al.[34] studied the lateral overgrowth of GaN and reported that the ratio of growth along the (002) and (100) surface normals varies significantly with deposition parameters such as the substrate temperature. Similar results have been reported by other researchers[35,36]. This concept has been schematically demonstrated in Fig. 10, where the surface hillocks are shown to be comprised of $\{10\bar{1}0\}$ and (0001) planes. As shown, increasing the growth temperature affects the growth rate along $\{10\bar{1}0\}$ surface normals to a greater degree than the (0001) normal.

RSC Advances Accepted Manuscript

X-ray reflectometry (XRR) was used to probe the structure of the thin films. Fig. 11 shows XRR curves of ALD GaN thin films deposited at various temperatures. For samples deposited at lower temperatures Kiessig fringes can be clearly observed. The distance between two consecutive peaks is indicative of the film thickness, while roughness and density mainly change the mean intensity and the intensity fluctuation amplitude. The gradual disappearance of Kiessig fringes might be the result of the increasing roughness. This trend agrees with the variation of roughness, as shown in Fig. 8 up to 360°C. It can be seen that even at 360°C traces of Kiessig fringes are detectable at lower angles, but the 425° sample shows a completely smooth curve, in spite of the fact that the roughness actually decreases above 360°C, as shown previously in Fig. 8. If surface roughness were the sole cause of waning Kiessig fringes, the faint intensity fluctuations at lower 2θ angles observed at deposition temperature of 360° would amplify when the substrate temperature is further heated to 425°C, as the surface roughness decreases. However, the sample deposited at 425° shows the absence of any such fluctuations. The simultaneous occurrence of the two seemingly contradictory observations necessitates the presence of a rival mechanism.

It has been repeatedly demonstrated that exposure of sapphire (001) surface to nitrogen plasma leads to formation of a nitride layer. The formation of this layer has been demonstrated using XPS[37–39], RHEED[40], and AFM[37,41]. The existence of such a layer means a gradual transition from Al_2O_3 to GaN, and the absence of a sharp interface. Kiessig fringes emerge after reflection of X-rays from a well-defined interface, whose absence disallows their existence. Since all the films were exposed to N_2/H_2 plasma for one minute prior to the start of deposition, formation of this transition AlN layer seems to be a likely contributor to the waning of the Kiessig fringes. Due to the rapid attenuation of the Kiessig fringes, a reliable simulation could not be performed for the

RSC Advances Accepted Manuscript

films deposited at higher temperatures, and the extraction of mass density from the XRR data requires another method. It is known that with increasing X-ray angle of incidence, there is a critical angle, at which the X-rays start penetrating the surface of the sample, and this angle is proportional to the square root of mass density of the film[42]. Using the critical angle, the relative density of the films was derived and plotted versus deposition temperature in Fig. 12. The first minimum in the second derivative of intensity was regarded as the threshold of X-ray penetration. The unit relative density in Fig. 12 corresponds to 5.96 gcm^{-3}, which is 97% of the bulk density. It is observed that at the deposition temperature of 240°C, the mass density reaches the relative value of 0.98, and no meaningful change occurs at higher temperatures.

3.4. Electrical and Optical Properties

Hall mobility measurements were conducted on the ALD GaN samples, and the results are shown in Fig. 13, where increasing the deposition temperature results in a decrease in resistivity and an increase in Hall mobility. Increasing the deposition temperature from 150°C to 425°C elevates Hall mobility from 2.2 to 575 cm^2/Vs, and decreases the resistivity from 3.7 to 0.007 Ωcm. The Hall mobility measured at 425°C is higher than what has been reported in several studies for thicker films deposited using CVD[43–46] and MBE[47] at higher temperatures. The increasing mobility versus substrate temperature, which has also been reported for CVD-grown GaN at temperatures above 1000°C [46], could be attributed to the increasing density, increasing crystallite size, and improving crystal quality, as discussed in Section 3.2. Crystal defects are known to adversely affect both mobility and conductivity, as they scatter the charge carriers[46,48,49]. Similar relationships between crystal structure and carrier mobility has also been reported by other researchers[16,50]. Cheng et al.[12] reported that increasing the substrate

RSC Advances Accepted Manuscript

temperature from 300° to 500°C during the atomic layer deposition of TiN results in a drop in resistivity by two orders of magnitude. A simultaneous increase in crystal order has also been reported by the authors. It is noteworthy that the films registered as p-type in our measurements.

The variation of the optical properties of the ALD GaN films was investigated using in-situ ellipsometry during growth at different temperatures. The refractive index was a function of thickness for all growth temperatures: a sharp drop was observed during the first initial ~100 cycles, before it starts increasing (Fig. 14a). This behavior has been reported earlier by the authors, and analyzed in view of TEM studies[51]. In short, the layers close to the interface are made up of higher quality crystal, and this phenomenon is reflected in the optical performance of the films. This is particularly noticeable, when compared to the results of a similar study performed on AlN films, deposited through a similar method[52]. The variation in the refractive index of the films, after 1000 cycles of deposition, at various temperatures is shown in Fig. 14b. The data are the results of ex-situ measurements at room temperature. Three temperature zones are identified on the graph: in zones I and II the refractive index increases with increasing temperature, while a sudden jump is observed between the two. In zone III, the index reaches a plateau, and is no longer dependent on the temperature. The variations in the refractive index can be analyzed for the three different temperature zones. In Zone I, below 240°C, the refractive index shows a steady increase. In this zone, the rise of refractive index is due to the increase in mass density (Fig. 12). Between 240°C and 275°C a sudden jump is observed. Fig. 3 shows that 275°C is the onset of crystallinity. Therefore this jump can be attributed to the difference between the optical properties of amorphous and crystalline GaN. Reports on the effect of crystallinity on the refractive index of semiconductors have been published before[53–55]. It was shown that larger grain size and higher quality crystallites, as manifested in XRD patterns, leads

RSC Advances Accepted Manuscript

to higher refractive index. As Fig. 3 shows, the diffraction patterns of the crystals are more pronounced, as the deposition temperature rises. This leads to an increase in the refractive index up until the deposition temperature of 360°C, as shown in Fig. 14b. The range of temperature spanning from 275° to 360°C has therefore been designated as zone II, in which crystal quality determines the refractive index. Temperatures above 360°C have been designated as zone III, where the increase of temperature does not affect the refractive index of GaN.

4. Conclusions

Substrate temperature was found to have a crucial role in all aspects of growth, structural evolution, electrical and optical properties of GaN films grown by atomic layer deposition. The films were found to be amorphous at temperatures of 240°C and below. XRD indicated that crystal quality improves at higher temperatures, owing to larger grain size and the optimal (002) orientation which occurs at 275°C and above. In addition, clear proof of the crystallographic relationship between the substrate and the films was observed for all the crystalline films. The combination of spectroscopic ellipsometry and AFM results strongly implies that a secondary growth mechanism is activated at 425°C. This leads to a substantial increase in growth rate, and a lower surface roughness. XRR analyses show that the characteristic Kiessig fringes gradually disappear at higher temperatures, regardless of the trends in variation of roughness. This is likely to be due to the formation of a thin AlN interlayer at the interface of the substrate and the film. Variation of the refractive index is a function of both film density and crystal structure, with a pronounced increase at the onset of crystallinity. Significant improvements of more than two orders of magnitude were observed in film conductivity and Hall mobility, when the substrate

RSC Advances Accepted Manuscript

temperature was increased from 150°C to 425°C. Under optimal growth conditions, PEALD GaN films grown on (002) sapphire were p-type with a hole mobility of 575 cm^2/vs.

References

(1) Ni, X.; Fu, Y.; Moon, Y. T.; Biyikli, N.; Morkoç, H. Optimization of a-Plane GaN Growth by MOCVD on R-Plane Sapphire. *J. Cryst. Growth* **2006**, *290*, 166–170.

(2) Arslan, E.; Ozturk, M. K.; Teke, A.; Ozcelik, S.; Ozbay, E. Buffer Optimization for Crack-Free GaN Epitaxial Layers Grown on Si(1 1 1) Substrate by MOCVD. *J. Phys. D. Appl. Phys.* **2008**, *41*, 155317.

(3) Imer, B.; Wu, F.; Craven, M. D.; Speck, J. S.; DenBaars, S. P. Stability of (1\bar100) M -Plane GaN Films Grown by Metalorganic Chemical Vapor Deposition. *Jpn. J. Appl. Phys.* **2006**, *45*, 8644–8647.

(4) Knox-Davies, E. C.; Shannon, J. M.; Silva, S. R. P. The Properties and Deposition Process of GaN Films Grown by Reactive Sputtering at Low Temperatures. *J. Appl. Phys.* **2006**, *99*, 073503.

(5) Junaid, M.; Hsiao, C.-L.; Palisaitis, J.; Jensen, J.; Persson, P. O. å.; Hultman, L.; Birch, J. Electronic-Grade GaN(0001)/Al2O3(0001) Grown by Reactive DC-Magnetron Sputter Epitaxy Using a Liquid Ga Target. *Appl. Phys. Lett.* **2011**, *98*, 141915.

(6) Calarco, R.; Meijers, R. J.; Debnath, R. K.; Stoica, T.; Sutter, E.; Lu, H. Nucleation and Growth of GaN Nanowires on Si (111) Performed by Molecular Beam Epitaxy. *Nano Lett.* **2007**, *7*, 2248–2251.

(7) Debnath, R. K.; Meijers, R.; Richter, T.; Stoica, T.; Calarco, R.; Lüth, H. Mechanism of Molecular Beam Epitaxy Growth of GaN Nanowires on Si(111). *Appl. Phys. Lett.* **2007**, *90*, 123117.

(8) Li, G.; Ohta, J.; Okamoto, K.; Kobayashi, A.; Fujioka, H. Room-Temperature Epitaxial Growth of GaN on Atomically Flat MgAl 2 O 4 Substrates by Pulsed-Laser Deposition. *Jpn. J. Appl. Phys.* **2006**, *45*, L457–L459.

(9) Kawaguchi, Y.; Ohta, J.; Kobayashi, a.; Fujioka, H. Room-Temperature Epitaxial Growth of GaN on Lattice-Matched ZrB[sub 2] Substrates by Pulsed-Laser Deposition. *Appl. Phys. Lett.* **2005**, *87*, 221907.

(10) Johnson, R. W.; Hultqvist, A.; Bent, S. F. A Brief Review of Atomic Layer Deposition: From Fundamentals to Applications. *Mater. Today* **2014**, *17*, 236–246.

(11) George, S. M. Atomic Layer Deposition: An Overview. *Chem. Rev.* **2010**, *110*, 111–131.

RSC Advances Accepted Manuscript

(12) Cheng, H.-E.; Lee, W.-J.; Hsu, C.-M. The Effect of Deposition Temperature on the Properties of TiN Diffusion Barriers Prepared by Atomic Layer Chemical Vapor Deposition. *Thin Solid Films* **2005**, *485*, 59–65.

(13) King, P. J.; Werner, M.; Chalker, P. R.; Jones, a. C.; Aspinall, H. C.; Basca, J.; Wrench, J. S.; Black, K.; Davies, H. O.; Heys, P. N. Effect of Deposition Temperature on the Properties of CeO2 Films Grown by Atomic Layer Deposition. *Thin Solid Films* **2011**, *519*, 4192–4195.

(14) Kukli, K.; Ritala, M.; Aarik, J.; Uustare, T.; Leskelä, M. Influence of Growth Temperature on Properties of Zirconium Dioxide Films Grown by Atomic Layer Deposition. *J. Appl. Phys.* **2002**, *92*, 1833.

(15) Lee, J.; Lee, S. J.; Han, W. B.; Jeon, H.; Park, J.; Jang, W.; Yoon, C. S.; Jeon, H. Deposition Temperature Dependence of Titanium Oxide Thin Films Grown by Remote-Plasma Atomic Layer Deposition. *Phys. Status Solidi* **2013**, *210*, 276–284.

(16) Makino, H.; Miyake, A.; Yamada, T.; Yamamoto, N.; Yamamoto, T. Influence of Substrate Temperature and Zn-Precursors on Atomic Layer Deposition of Polycrystalline ZnO Films on Glass. *Thin Solid Films* **2009**, *517*, 3138–3142.

(17) Yuan, N. Y.; Wang, S. Y.; Tan, C. B.; Wang, X. Q.; Chen, G. G.; Ding, J. N. The Influence of Deposition Temperature on Growth Mode, Optical and Mechanical Properties of ZnO Films Prepared by the ALD Method. *J. Cryst. Growth* **2013**, *366*, 43–46.

(18) Särkijärvi, S.; Sintonen, S.; Tuomisto, F.; Bosund, M.; Suihkonen, S.; Lipsanen, H. Effect of Growth Temperature on the Epitaxial Growth of ZnO on GaN by ALD. *J. Cryst. Growth* **2014**, *398*, 18–22.

(19) Ozgit, C.; Donmez, I.; Alevli, M.; Biyikli, N. Atomic Layer Deposition of GaN at Low Temperatures. *J. Vac. Sci. Technol. A Vacuum, Surfaces, Film.* **2012**, *30*, 01A124.

(20) Kim, O. H.; Kim, D.; Anderson, T. Atomic Layer Deposition of GaN Using GaCl[sub 3] and NH[sub 3]. *J. Vac. Sci. Technol. A Vacuum, Surfaces, Film.* **2009**, *27*, 923.

(21) Ozgit-Akgun, C.; Goldenberg, E.; Okyay, A. K.; Biyikli, N. Hollow Cathode Plasma-Assisted Atomic Layer Deposition of Crystalline AlN, GaN and AlxGa1−xN Thin Films at Low Temperatures. *J. Mater. Chem. C* **2014**, *2*, 2123.

(22) Foroughi-Abari, A.; Cadien, K. C. In Situ Spectroscopic Ellipsometry Study of Plasma-Enhanced ALD of Al2O3 on Chromium Substrates. *J. Electrochem. Soc.* **2012**, *159*, D59.

(23) Birkholz, M. *Thin Film Analysis by X-Ray Scattering*; Wiley, 2006.

RSC Advances Accepted Manuscript

(24) Sayed, S. Y.; Buriak, J. M. Epitaxial Growth of Nanostructured Gold Films on Germanium via Galvanic Displacement. *ACS Appl. Mater. Interfaces* **2010**, *2*, 3515–3524.

(25) Nagata, T.; Volk, J.; Haemori, M.; Yamashita, Y.; Yoshikawa, H.; Hayakawa, R.; Yoshitake, M.; Ueda, S.; Kobayashi, K.; Chikyow, T. Schottky Barrier Height Behavior of Pt–Ru Alloy Contacts on Single-Crystal N-ZnO. *J. Appl. Phys.* **2010**, *107*, 103714.

(26) Moram, M. a.; Barber, Z. H.; Humphreys, C. J. Accurate Experimental Determination of the Poisson's Ratio of GaN Using High-Resolution X-Ray Diffraction. *J. Appl. Phys.* **2007**, *102*.

(27) Lim, J.; Lee, C. Effects of Substrate Temperature on the Microstructure and Photoluminescence Properties of ZnO Thin Films Prepared by Atomic Layer Deposition. *Thin Solid Films* **2007**, *515*, 3335–3338.

(28) Scarel, G.; Ferrari, S.; Spiga, S.; Wiemer, C.; Tallarida, G.; Fanciulli, M. Effects of Growth Temperature on the Properties of Atomic Layer Deposition Grown ZrO[sub 2] Films. *J. Vac. Sci. Technol. A Vacuum, Surfaces, Film.* **2003**, *21*, 1359.

(29) Brinks, P.; Heijmerikx, H.; Hendriks, T. a.; Rijnders, G.; Huijben, M. Achieving Chemical Stability in Thermoelectric NaxCoO2 Thin Films. *RSC Adv.* **2012**, *2*, 6023.

(30) Pitzer, K. S.; Brewer, L. Mass Spectrometric Study of Ga(CH3)3 and Ga(C2H5) 3 Decomposition Reaction in H2 and. *J. Electrochem. Soc. Solid-State Sci. Technol.* **1975**, *132*, 677–679.

(31) Oikawa, S.; Tsuda, M.; Morishita, M.; MASHITA, M.; Kuniya, Y. Elementary Process of the Thermal Decomposition of Alkyl Gallium. *J. Cryst. Growth* **1988**, *91*, 471–480.

(32) Donnelly, V. M.; McCaulley, J. A. Products of Thermal and Trimethylgallium Decomposition of Triethylgallium Adsorbed on Ga-Stabilized. *Surf. Sci.* **1990**, *238*, 34–52.

(33) McCaulley, J. a.; Shu, R. J.; Donnelly, V. M. Kinetics of Thermal Decomposition of Triethylgallium, Trimethylgallium, and Trimethylindium Adsorbed on GaAs(100). *J. Vac. Sci. Technol. A Vacuum, Surfaces, Film.* **1991**, *9*, 2872.

(34) Gu, S.; Zhang, R.; Shi, Y.; Zheng, Y. Epitaxial Lateral Overgrowth of GaN on Molecular Beam Epitaxy GaN Buffer Layers on Si Substrates by Hydride Vapour Phase Epitaxy. *J. Phys. D. Appl. Phys.* **2001**, *34*, 1951–1954.

(35) Kapolnek, D.; Keller, S.; Vetury, R.; Underwood, R. D.; Kozodoy, P.; Den Baars, S. P.; Mishra, U. K. Anisotropic Epitaxial Lateral Growth in GaN Selective Area Epitaxy. *Appl. Phys. Lett.* **1997**, *71*, 1204.

RSC Advances Accepted Manuscript

(36) Roskowski, a. M.; Miraglia, P. Q.; Preble, E. a.; Einfeldt, S.; Davis, R. F. Surface Instability and Associated Roughness during Conventional and Pendeo-Epitaxial Growth of GaN(0001) Films via MOVPE. *J. Cryst. Growth* **2002**, *241*, 141–150.

(37) Paek, J.-S.; Kim, K.-K.; Lee, J.-M.; Kim, D.-J.; Yi, M.-S.; Noh, D. Y.; Kim, H.-G.; Park, S.-J. Nitridation of Sapphire Substrate and Its Effect on the Growth of GaN Layer at Low Temperature. *J. Cryst. Growth* **1999**, *200*, 55–62.

(38) Losurdo, M.; Capezzuto, P.; Bruno, G. Plasma Cleaning and Nitridation of Sapphire (α-Al[sub 2]O[sub 3]) Surfaces: New Evidence from in Situ Real Time Ellipsometry. *J. Appl. Phys.* **2000**, *88*, 2138.

(39) Losurdo, M.; Capezzuto, P.; Bruno, G.; Namkoong, G.; Doolittle, W. A.; Brown, A. S. Role of Sapphire Nitridation Temperature on GaN Growth by Plasma Assisted Molecular Beam Epitaxy : Part II . Interplay between Chemistry and Structure of Layers Role of Sapphire Nitridation Temperature on GaN Growth by Plasma Assisted Molecular Beam Epita. *J. Appl. Phys.* **2002**, *91*, 2508–2518.

(40) Widmann, F.; Feuillet, G.; Daudin, B.; Rouvière, J. L. Low Temperature Sapphire Nitridation: A Clue to Optimize GaN Layers Grown by Molecular Beam Epitaxy. *J. Appl. Phys.* **1999**, *85*, 1550.

(41) Grandjean, N.; Massies, J.; Leroux, M. Nitridation of Sapphire. Effect on the Optical Properties of GaN Epitaxial Overlayers. *Appl. Phys. Lett.* **1996**, *69*, 2071.

(42) Chason, E.; Mayer, T. M. Thin Film and Surface Characterization by Specular X-Ray Reflectivity. *Crit. Rev. Solid State Mater. Sci.* **1997**, *22*, 1–67.

(43) Meister, D.; Böhm, M.; Topf, M.; Kriegseis, W.; Burkhardt, W.; Dirnstorfer, I.; Rösel, S.; Farangis, B.; Meyer, B. K.; Hoffmann, a.; *et al.* A Comparison of the Hall-Effect and Secondary Ion Mass Spectroscopy on the Shallow Oxygen Donor in Unintentionally Doped GaN Films. *J. Appl. Phys.* **2000**, *88*, 1811.

(44) Ko, C.-H.; Chang, S.-J.; Su, Y.-K.; Lan, W.-H.; Chen, J. F.; Kuan, T.-M.; Huang, Y.-C.; Chiang, C.-I.; Webb, J.; Lin, W.-J. On the Carrier Concentration and Hall Mobility in GaN Epilayers. *Jpn. J. Appl. Phys.* **2002**, *41*, L226–L228.

(45) Hwang, C. Y.; Schurman, M. J.; Mayo, W. E.; Lu, Y. C.; Stall, R. a.; Salagaj, T. Effect of Structural Defects and Chemical Impurities on Hall Mobilities in Low Pressure MOCVD Grown GaN. *J. Electron. Mater.* **1997**, *26*, 243–251.

(46) Wang, T.; Shirahama, T.; Sun, H. B.; Wang, H. X.; Bai, J.; Sakai, S.; Misawa, H. Influence of Buffer Layer and Growth Temperature on the Properties of an Undoped GaN Layer Grown on Sapphire Substrate by Metalorganic Chemical Vapor Deposition. *Appl. Phys. Lett.* **2000**, *76*, 2220.

RSC Advances Accepted Manuscript

(47) Kordoš, P.; Javorka, P.; Morvic, M.; Betko, J.; Van Hove, J. M.; Wowchak, a. M.; Chow, P. P. Conductivity and Hall-Effect in Highly Resistive GaN Layers. *Appl. Phys. Lett.* **2000**, *76*, 3762.

(48) Ahadi, K.; Nemati, A.; Mahdavi, S. M.; Vaezi, A. Effect of Simultaneous Chemical Substitution of A and B Sites on the Electronic Structure of BiFeO3 Films Grown on BaTiO 3/SiO2/Si Substrate. *J. Mater. Sci. Mater. Electron.* **2013**, *24*, 2128–2134.

(49) Ahadi, K.; Mahdavi, S.-M.; Nemati, A.; Tabesh, M.; Ranjbar, M. Electronic Structure and Morphological Study of BaTiO3 Film Grown by Pulsed-Laser Deposition. *Mater. Lett.* **2012**, *72*, 107–109.

(50) Ahn, C. H.; Lee, S. Y.; Cho, H. K. Influence of Growth Temperature on the Electrical and Structural Characteristics of Conductive Al-Doped ZnO Thin Films Grown by Atomic Layer Deposition. *Thin Solid Films* **2013**, *545*, 106–110.

(51) Motamedi, P.; Dalili, N.; Cadien, K. A Route to Low Temperature Growth of Single Crystal GaN on Sapphire. *J. Mater. Chem. C* **2015**, *In Press*.

(52) Motamedi, P.; Cadien, K. Structural and Optical Characterization of Low-Temperature ALD Crystalline AlN. *J. Cryst. Growth* **2015**, *421*, 45–52.

(53) Jakhar, A.; Jamdagni, A.; Bakshi, A.; Verma, T.; Shukla, V.; Jain, P.; Sinha, N.; Arun, P. Refractive Index of SnS Thin Nano-Crystalline Films. *Solid State Commun.* **2013**, *168*, 31–35.

(54) Fang, Z. B.; Yan, Z. J.; Tan, Y. S.; Liu, X. Q.; Wang, Y. Y. Influence of Post-Annealing Treatment on the Structure Properties of ZnO Films. *Appl. Surf. Sci.* **2005**, *241*, 303–308.

(55) Moustaghfir, A.; Tomasella, E.; Ben Amor, S.; Jacquet, M.; Cellier, J.; Sauvage, T. Structural and Optical Studies of ZnO Thin Films Deposited by R.f. Magnetron Sputtering: Influence of Annealing. *Surf. Coatings Technol.* **2003**, *174-175*, 193–196.

RSC Advances Accepted Manuscript

Figure Captions

Figure 1. ALD saturation curves for the triethylgallium and forming gas at 275°C deposition temperature and 600W plasma power; the curve at the top (blue) shows the effect of TEG pulse width on the growth rate, while plasma pulse width was kept constant at 15s; the curve at the bottom (red) shows the effect of plasma pulse width on the growth rate, while TEG pulse width was kept constant at 0.04s.

Figure 2. Schematic diagram illustrating the geometric variables of XRD test.

Figure 3. Two-dimensional XRD frames of 1000-cycle GaN films deposited at a) 150°C b) 200°C c) 240°C d) 275°C e) 325°C f) 360°C g) 425°C.

Figure 4. Integration of the diffraction intensity as a function of a) 2θ, b) χ for GaN films deposited at various substrate temperatures.

Figure 5. The azimuthal scans of sapphire (006) and GaN (002) deposited at 325°C.

Figure 6. Evolution of XRD rocking curves of the GaN (002) peak with increasing substrate temperature.

Figure 7. Growth rate of GaN as a function of growth temperature, and the inverse of absolute temperature, plotted in terms of absolute growth rate and the number of monolayers grown in every deposition cycle.

Figure 8. Variations of GaN surface roughness vs deposition temperature.

Figure 9. AFM images of 1000 cycle-grown GaN films with the substrate temperature of a) 150°C b) 325°C c) 425°C.

RSC Advances Accepted Manuscript

Figure 10. Schematic diagram illustrating the effect of substrate temperature on the lateral and longitudinal growth rates of GaN hillocks. Blue and red arrows indicate lower and higher temperature, respectively.

Figure 11. X-ray reflectometry spectra of GaN films deposited at various temperatures.

Figure 12. Variations of the mass density as a function of the growth temperature. The numbers are normalized to the maximum observed density.

Figure 13. The dependence of resistivity and carrier mobility on the substrate temperature.

Figure 14. a) The in-situ observation of the evolution of refractive index at 632 nm, plotted at two representative temperatures, b) The dependence of refractive index on the growth temperature, plotted at three different representative wavelengths with three different zones designated based on the behavior of the refractive index.

RSC Advances Accepted Manuscript

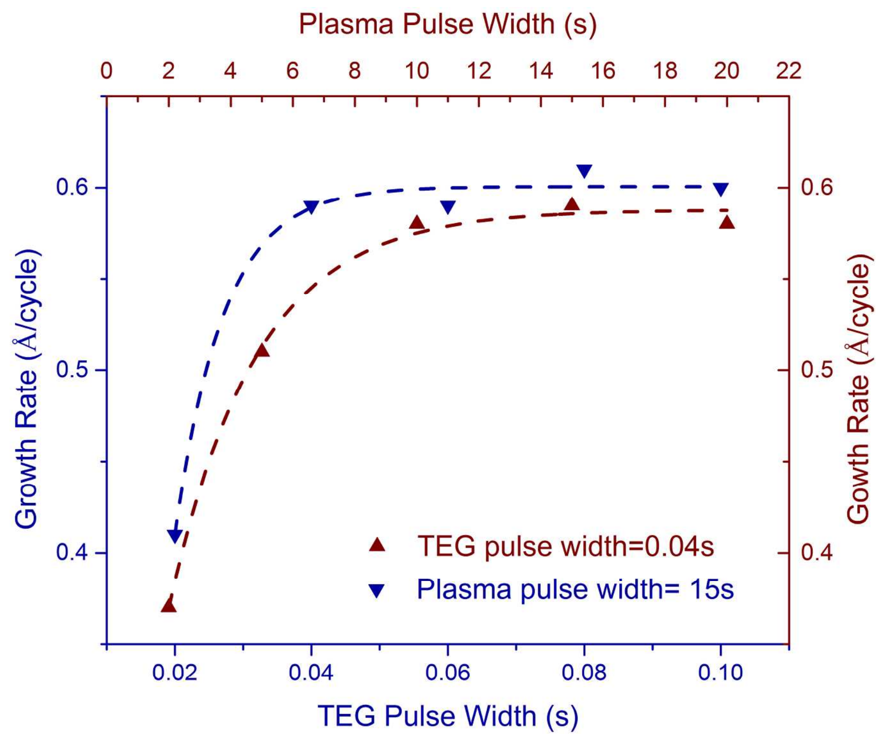

207x158mm (300 x 300 DPI)

RSC Advances Accepted Manuscript

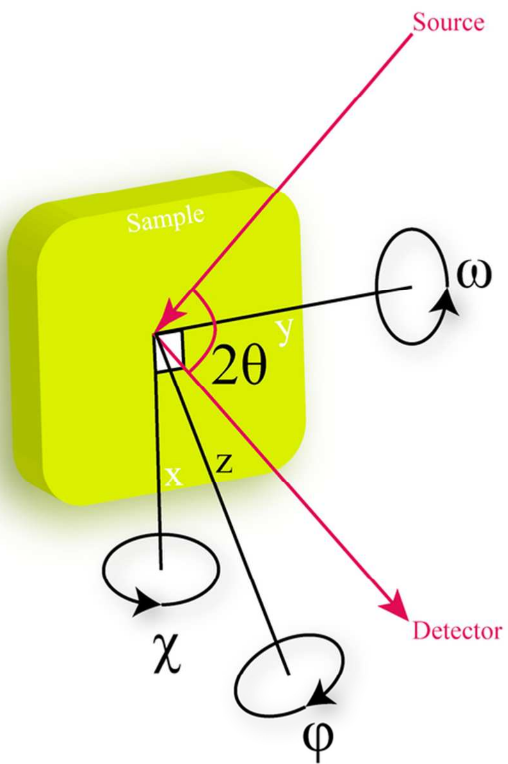

82x63mm (300 x 300 DPI)

RSC Advances Accepted Manuscript

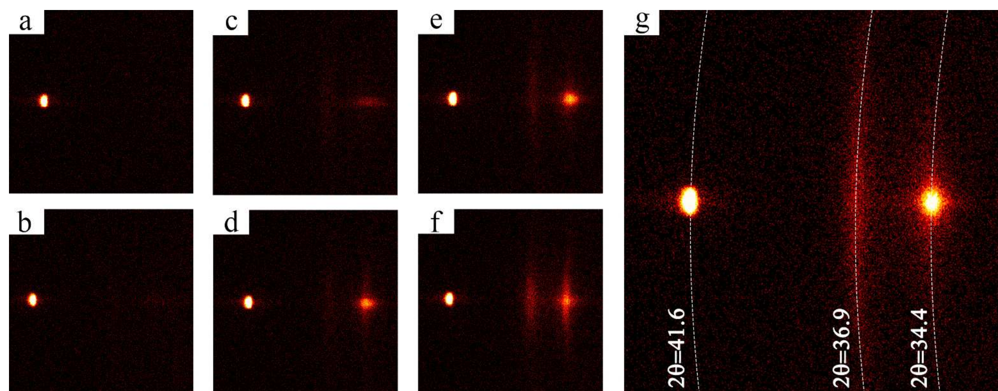

233x89mm (300 x 300 DPI)

RSC Advances Accepted Manuscript

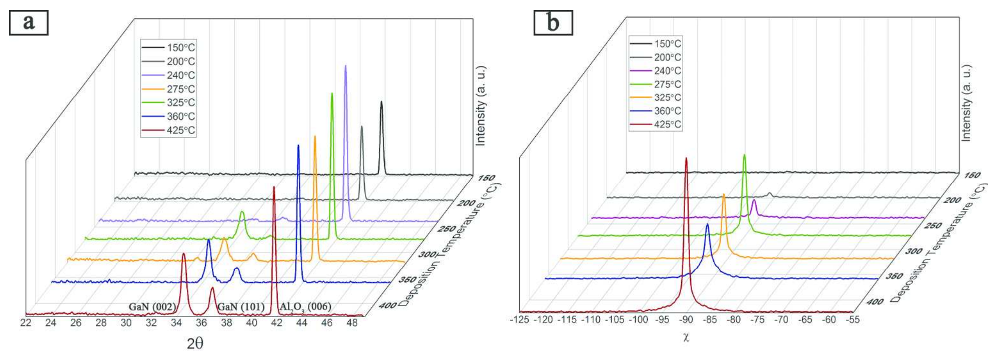

203x70mm (300 x 300 DPI)

RSC Advances Accepted Manuscript

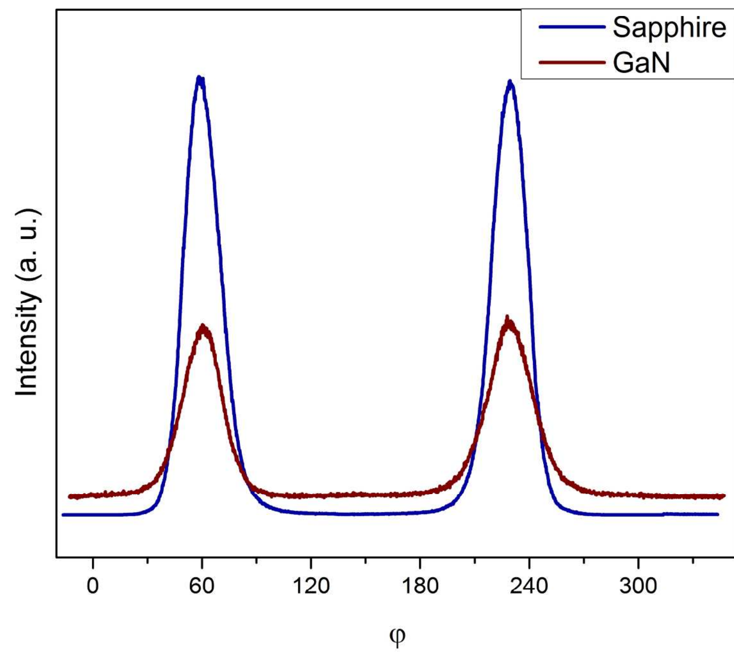

207x158mm (300 x 300 DPI)

RSC Advances Accepted Manuscript

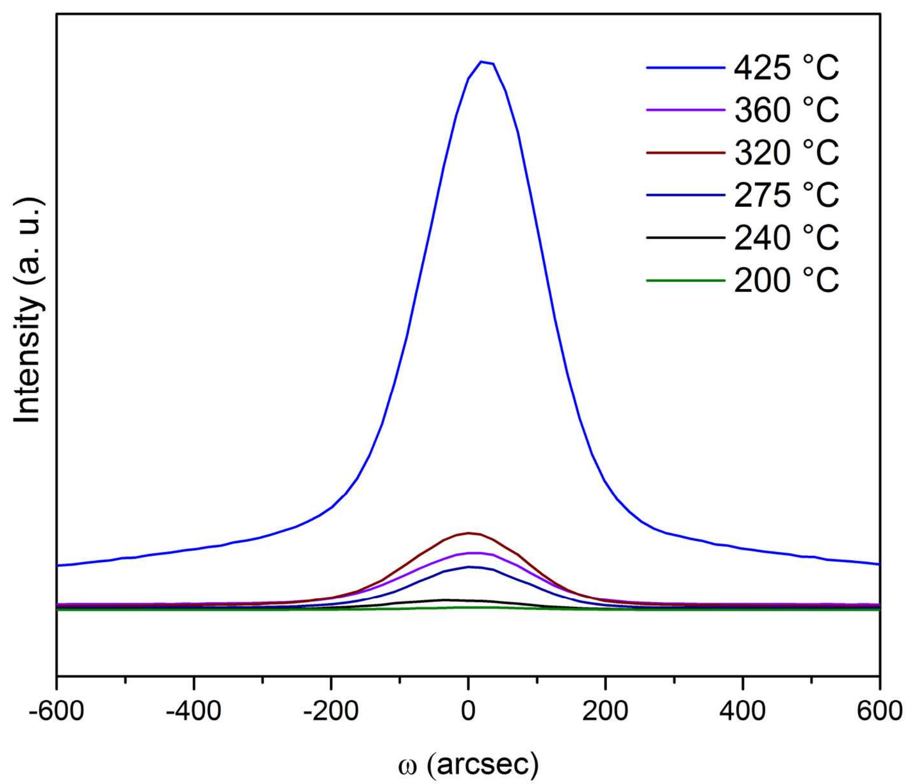

184x152mm (300 x 300 DPI)

RSC Advances Accepted Manuscript

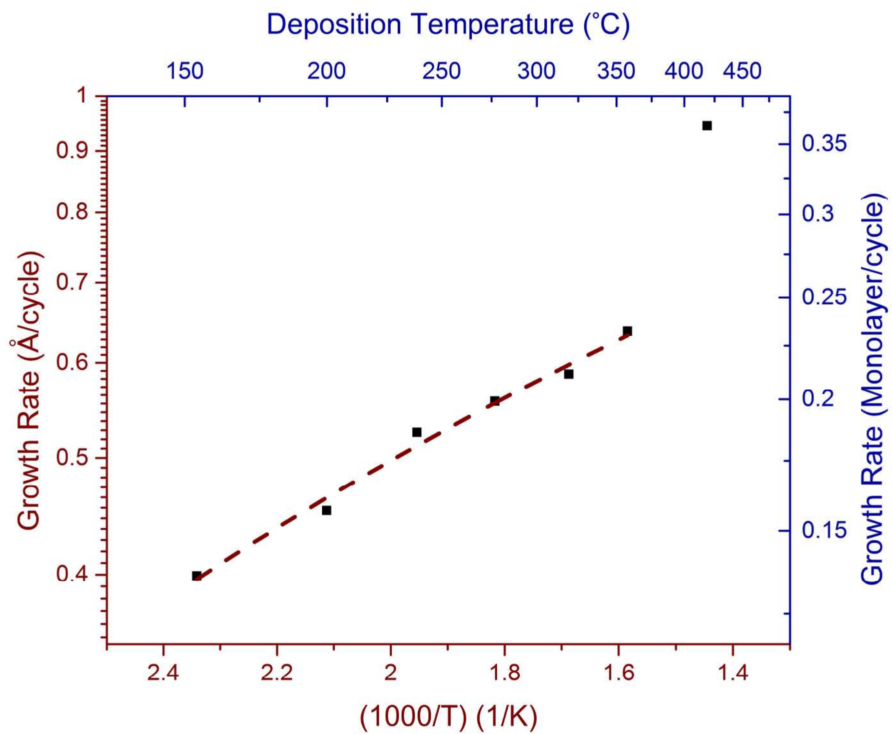

207x158mm (300 x 300 DPI)

RSC Advances Accepted Manuscript

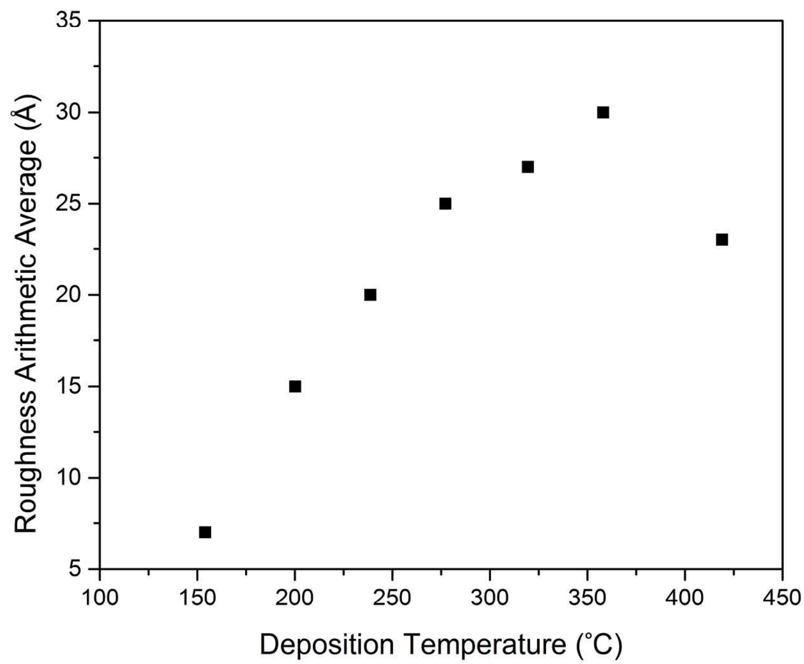

207x158mm (300 x 300 DPI)

RSC Advances Accepted Manuscript

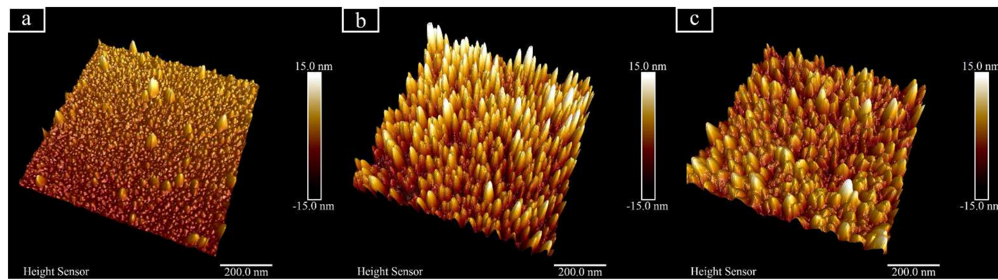

380x103mm (300 x 300 DPI)

RSC Advances Accepted Manuscript

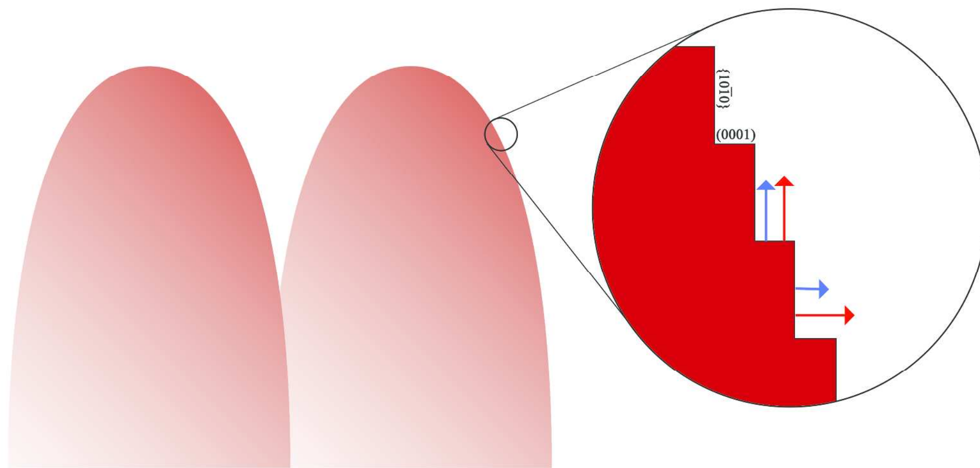

250x123mm (300 x 300 DPI)

RSC Advances Accepted Manuscript

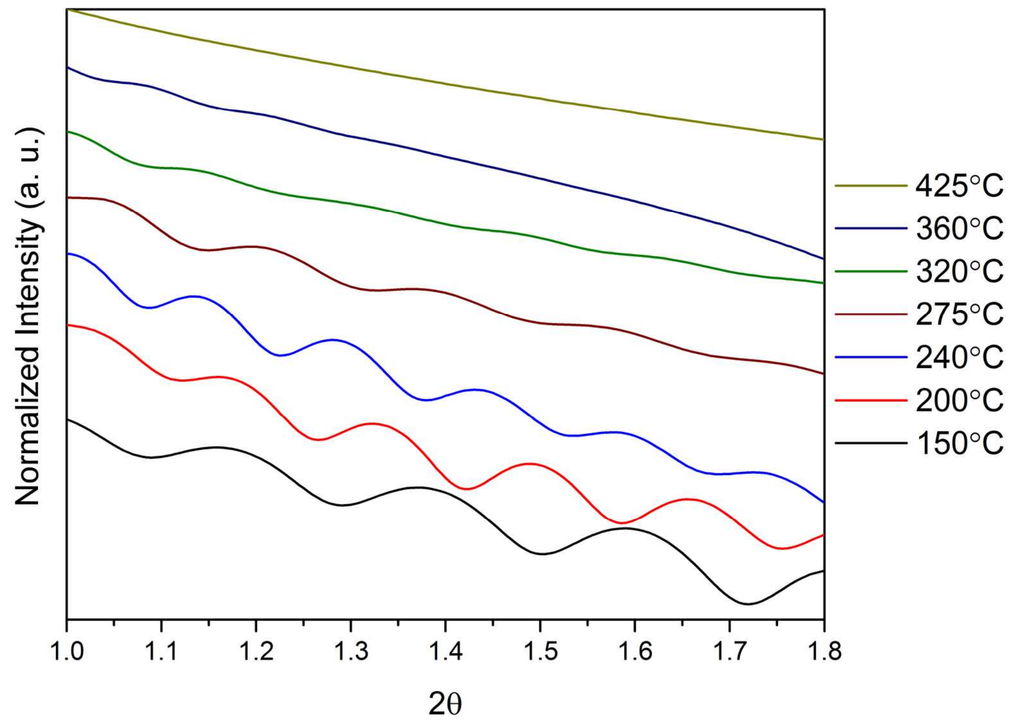

174x125mm (300 x 300 DPI)

RSC Advances Accepted Manuscript

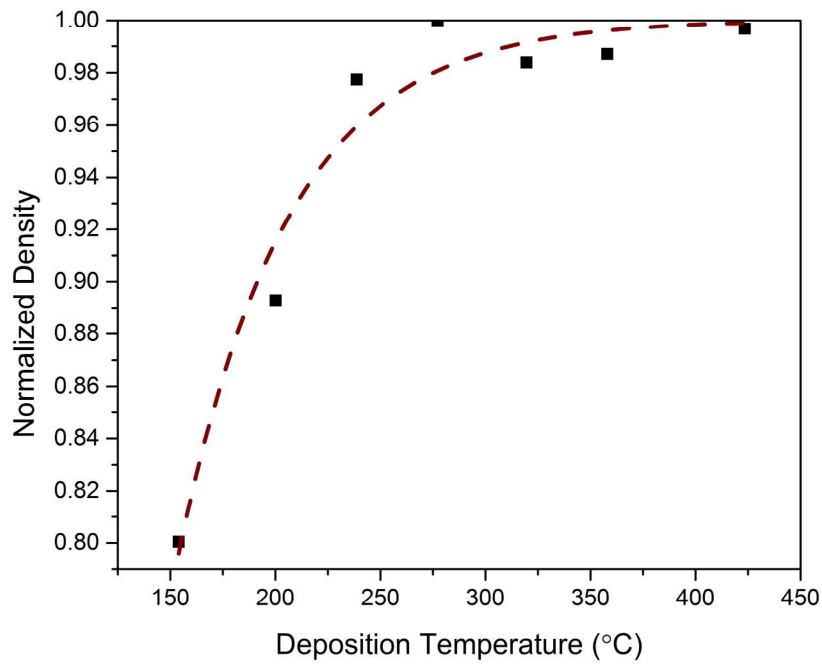

207x158mm (300 x 300 DPI)

RSC Advances Accepted Manuscript

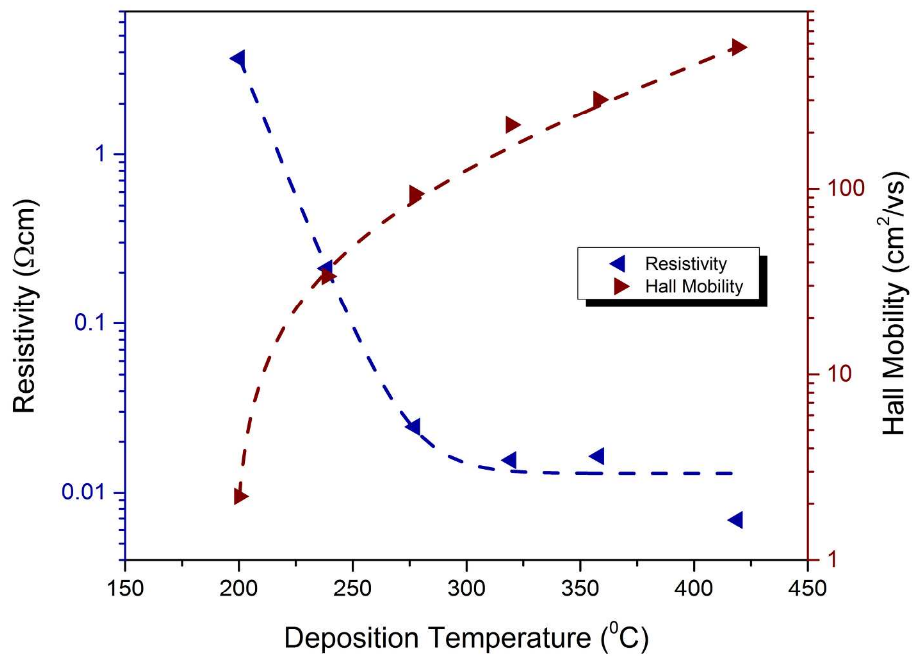

207x158mm (300 x 300 DPI)

RSC Advances Accepted Manuscript

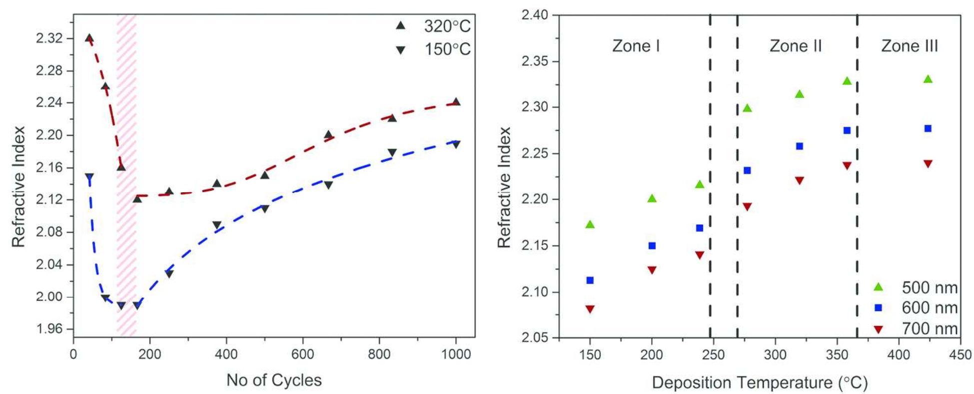

172x72mm (300 x 300 DPI)

RSC Advances Accepted Manuscript